2530 *Inorg. Chem.* **2010**, *49*, 2530–2540
DOI: 10.1021/ic902465b

Inorganic Chemistry
Article

Structure, Photophysical and Electrochemical Properties, Biomolecular Interactions, and Intracellular Uptake of Luminescent Cyclometalated Iridium(III) Dipyridoquinoxaline Complexes

Kenneth Yin Zhang,[†] Steve Po-Yam Li,[†] Nianyong Zhu,[‡] Iyana Wai-Shan Or,[†] Maggie Shau-Ha Cheung,[†] Yun-Wah Lam,*[,†] and Kenneth Kam-Wing Lo*[,†]

[†]*Department of Biology and Chemistry, City University of Hong Kong, Tat Chee Avenue, Kowloon, Hong Kong, P.R. China, and* [‡]*Department of Chemistry, The University of Hong Kong, Pokfulam Road, Hong Kong, P.R. China*

Received December 12, 2009

A series of luminescent cyclometalated iridium(III) dipyridoquinoxaline complexes $[Ir(N^{\wedge}C)_2(N^{\wedge}N)](PF_6)$ ($HN^{\wedge}C$ = 1-phenylpyrazole, Hppz, $N^{\wedge}N$ = dipyrido[3,2-*f*:2′,3′-*h*]quinoxaline, dpq (**1a**), 2-(*n*-butylamido)dipyrido-[3,2-*f*:2′,3′-*h*]quinoxaline, dpqa (**1b**); $HN^{\wedge}C$ = 7,8-benzoquinoline, Hbzq, $N^{\wedge}N$ = dpq (**2a**), dpqa (**2b**); $HN^{\wedge}C$ = 2-phenylquinoline, Hpq, $N^{\wedge}N$ = dpq (**3a**), dpqa (**3b**)) has been synthesized and characterized. Cyclic voltammetric studies revealed a reversible or quasi-reversible iridium(IV/III) oxidation couple at about +1.13 to +1.32 V and a reversible diimine reduction couple at about −1.10 to −1.29 V versus SCE. Upon photoexcitation, all the complexes displayed intense and long-lived green to orange triplet metal-to-ligand charge-transfer (^{3}MLCT) ($d\pi(Ir) \rightarrow \pi^*$(dpq or dpqa)) emission in aprotic organic solvents at room temperature and in low-temperature glass. In aqueous solution, these complexes were only weakly emissive or even non-emissive. The lipophilicity of all the complexes has been determined by reversed-phase HPLC. The cytotoxicity of these iridium(III) complexes toward the human cervix epithelioid carcinoma (HeLa) and Madin-Darby canine kidney (MDCK) cell lines has been evaluated by the 3-(4,5-dimethyl-2-thiazolyl)-2,5-diphenyltetrazolium bromide (MTT) assay. The cellular uptake of the complexes by MDCK cells has been examined by laser-scanning confocal microscopy. Most importantly, apparent nucleolar staining was observed after the cells were treated by the complexes. The interactions of these complexes with proteins, DNA, and RNA have also been studied by emission titrations and SDS-PAGE gel staining. The results revealed that the complexes bound to the hydrophobic pockets of proteins, intercalated into the base-pairs of double-stranded DNA, but did not appear to interact with RNA.

Introduction

The development of cellular probes is important and essential to understanding the diverse structures and functions of biological systems. Fluorescent or luminescent cellular probes derived from organic dyes,[1] quantum dots,[2] and lanthanide chelates[3] have been extensively studied. By virtue of their highly environment-sensitive emissive behavior and diverse excited-state character, luminescent transition metal polypyridine complexes have been widely utilized as molecular probes for nucleic acids, peptides, and proteins.[4−7] These luminescent probes often provide information of their local environment through a change of their emission intensity, wavelength, and lifetime. There has been an emerging interest in applying luminescent inorganic and organometallic complexes to investigating

*To whom correspondence should be addressed. E-mail: yunwlam@cityu.edu.hk (Y.-W.L.), bhkenlo@cityu.edu.hk (K.K.-W.L.). Phone: (852) 2788 7231. Fax: (852) 2788 7406.

(1) See, for example, Haugland, R. P. *The Handbook−A Guide to Fluorescent Probes and Labeling Technologies*, 10th ed.; Molecular Probes, Inc.: Eugene, OR, 2005; Chapters 8−14.

(2) See, for example, (a) Gao, X.; Yang, L.; Petros, J. A.; Marshall, F. F.; Simons, J. W.; Nie, S. *Curr. Opin. Biotechnol.* **2005**, *16*, 63–72. (b) Alivisatos, A. P.; Gu, W.; Larabell, C. *Annu. Rev. Biomed. Eng.* **2005**, *7*, 55–76. (c) Smith, A. M.; Duan, H.; Mohs, A. M.; Nie, S. *Adv. Drug Delivery Rev.* **2008**, *60*, 1226–1240.

(3) See, for example, (a) Montgomery, C. P.; Murray, B. S.; New, E. J.; Pal, R.; Parker, D. *Acc. Chem. Res.* **2009**, *42*, 925–927. (b) Chauvin, A.-S.; Comby, S.; Song, B.; Vandevyver, C. D. B.; Bünzli, J.-C. G. *Chem.—Eur. J.* **2008**, *14*, 1726–1739.

(4) Terpetschnig, E.; Szmacinski, H.; Lakowicz, J. R. *Methods Enzymol.* **1997**, *278*, 295–321.

(5) Erkkila, K. E.; Odom, D. T.; Barton, J. K. *Chem. Rev.* **1999**, *99*, 2777–2795.

(6) Pierard, F.; Kirsch-De Mesmaeker, A. *Inorg. Chem. Commun.* **2006**, *9*, 111–126.

(7) Lo, K. K.-W. *Struct. Bonding* (*Berlin*) **2007**, *123*, 205–245.

Published on Web 02/04/2010

cellular systems; for example, luminescent platinum(II),[8,9] ruthenium(II),[10−14] zinc(II),[15] rhenium(I),[16−18] rhodium(III),[19] and iridium(III)[20,21] complexes have been used as intracellular probes and biological imaging reagents for live cells. Despite these reports, binding of luminescent transition metal complexes to the nucleus or nuclear components remains relatively unexplored.[15b] Recently, rhodium(III) and ruthenium(II) complexes appended with a fluorescein and phenanthridine unit have been found to stain the nucleoli of mammalian cells.[11c,12,19] However, the nuclear uptake and staining rely heavily on the oligopeptide spacer and/or the organic pendants in these systems.[11c,12,19]

With our ongoing interest in luminescent iridium(III) polypyridine complexes as biological labels and probes,[21,22] we envisage that cyclometalated iridium(III) polypyridine complexes containing an intercalating ligand have a high potential to serve as new luminescent probes for biological molecules and live cells. Previously, we have studied the DNA-binding properties of cyclometalated iridium(III)-based metallointercalators.[22c] In this work, we report a new series of iridium(III) dipyridoquinoxaline complexes $[Ir(N^{\wedge}C)_2(N^{\wedge}N)](PF_6)$ (HN^C = 1-phenylpyrazole, Hppz, N^N = dipyrido[3,2-*f*:2′,3′-*h*]quinoxaline, dpq (**1a**), 2-(*n*-butylamido)dipyrido[3,2-*f*:2′,3′-*h*]quinoxaline, dpqa (**1b**); HN^C = 7,8-benzoquinoline, Hbzq, N^N = dpq (**2a**), dpqa (**2b**); HN^C = 2-phenylquinoline, Hpq, N^N = dpq (**3a**), dpqa (**3b**)) (Chart 1). The properties, including the lipophilicity, of these complexes have been changed by using cyclometalating ligands of different hydrophobicity. The reason for using the dpqa ligand in additional to the dpq ligand is that its amide unit effectively suppresses the emission of the iridium(III) complexes in aqueous solution but allows them to emit strongly in organic solvents or when bound to biomolecules, resulting in excellent detection sensitivity.[22c,23] The cytotoxicity and cellular uptake properties of these complexes have been studied using the human cervix epithelioid carcinoma (HeLa) and Madin-Darby canine kidney (MDCK) as model cell lines. Importantly, we found that all the complexes stained the nucleoli of the MDCK cells. The possible interactions of these complexes with the proteins, DNA, and RNA have also been studied by emission titrations and SDS-PAGE gel staining.

Chart 1. Structures of the Iridium(III) Dpq and Dpqa Complexes

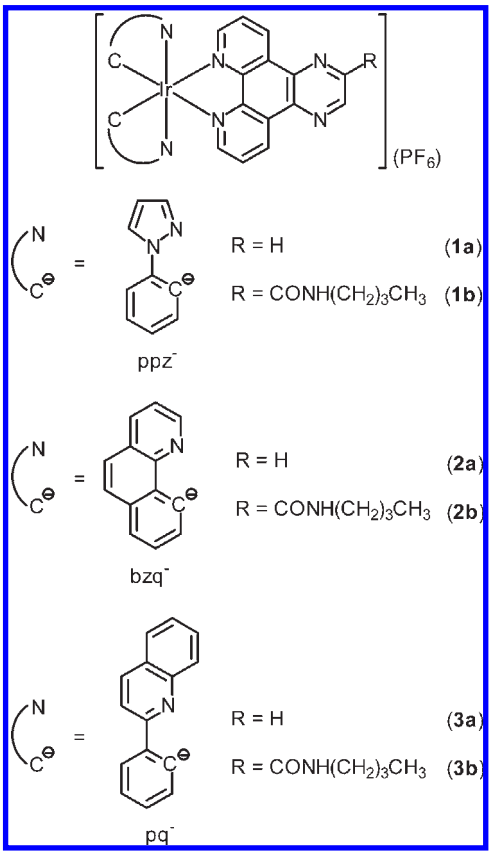

Results and Discussion

Synthesis. All the complexes were synthesized from the reaction of the iridium dimer $[Ir_2(N^{\wedge}C)_4Cl_2]$ with the diimine ligand dpq or dpqa, purified by column chromatography, recrystallized from acetone/diethyl ether, and isolated as yellow to orange-red crystals. They showed good solubility in common organic solvents and aqueous DMSO and MeOH solutions.

(8) Botchway, S. W.; Charnley, M.; Haycock, J. W.; Parker, A. W.; Rochester, D. L.; Weinstein, J. A.; Williams, J. A. G. *Proc. Natl. Acad. Sci. U.S.A.* **2008**, *105*, 16071–16076.
(9) Wu, P.; Wong, E. L.-M.; Ma, D. L.; Tong, G. S.-M.; Ng, K.-M.; Che, C.-M. *Chem.—Eur. J.* **2009**, *15*, 3652–3656.
(10) Önfelt, B.; Göstring, L.; Lincoln, P.; Nordén, B.; Önfelt, A. *Mutagenesis* **2002**, *17*, 317–320.
(11) (a) Puckett, C. A.; Barton, J. K. *J. Am. Chem. Soc.* **2007**, *129*, 46–47. (b) Puckett, C. A.; Barton, J. K. *Biochemistry* **2008**, *47*, 11711–11716. (c) Puckett, C. A.; Barton, J. K. *J. Am. Chem. Soc.* **2009**, *131*, 8738–8739.
(12) O'Connor, N. A.; Stevens, N.; Samaroo, D.; Solomon, M. R.; Martí, A. A.; Dyer, J.; Vishwasrao, H.; Akins, D. L.; Kandel, E. R.; Turro, N. J. *Chem. Commun.* **2009**, 2640–2642.
(13) Neugebauer, U.; Pellegrin, Y.; Devocelle, M.; Forster, R. J.; Signac, W.; Morand, N.; Keyes, T. E. *Chem. Commun.* **2008**, 5307–5309.
(14) Lo, K. K.-W.; Lee, T. K.-M.; Lau, J. S.-Y.; Poon, W.-L.; Cheng, S.-H. *Inorg. Chem.* **2008**, *47*, 200–208.
(15) (a) Pascu, S. I.; Waghorn, P. A.; Conry, T. D.; Lin, B.; Betts, H. M.; Dilworth, J. R.; Sim, R. B.; Churchill, G. C.; Aigbirhio, F. I.; Warren, J. E. *Dalton Trans.* **2008**, 2107–2110. (b) During the preparation of this manuscript, an interesting paper about the nucleolus-staining properties of zinc-Triapine complexes was published: Kowol, C. R.; Trondl, R.; Arion, V. B.; Jakupec, M. A.; Lichtscheidl, I.; Keppler, B. K. *Dalton Trans.* **2010**, *39*, 704–706.
(16) Stephenson, K. A.; Banerjee, S. R.; Besanger, T.; Sogbein, O. O.; Levadala, M. K.; McFarlane, N.; Lemon, J. A.; Boreham, D. R.; Maresca, K. P.; Brennan, J. D.; Babich, J. W.; Zubieta, J.; Valliant, J. F. *J. Am. Chem. Soc.* **2004**, *126*, 8598–8599.
(17) (a) Amoroso, A. J.; Coogan, M. P.; Dunne, J. E.; Fernández-Moreira, V.; Hess, J. B.; Hayes, A. J.; Lloyd, D.; Millet, C.; Pope, S. J. A.; Williams, C. *Chem. Commun.* **2007**, 3066–3068. (b) Amoroso, A. J.; Arthur, R. J.; Coogan, M. P.; Court, J. B.; Fernández-Moreira, V.; Hayes, A. J.; Lloyd, D.; Millet, C.; Pope, S. J. A. *New J. Chem.* **2008**, *32*, 1097–1102.
(18) (a) Lo, K. K.-W.; Louie, M.-W.; Sze, K.-S.; Lau, J. S.-Y. *Inorg. Chem.* **2008**, *47*, 602–611. (b) Louie, M.-W.; Liu, H.-W.; Lam, M. H.-C.; Lau, T.-C.; Lo, K. K.-W. *Organometallics* **2009**, *28*, 4297–4307. (c) Louie, M.-W.; Lam, M. H.-C.; Lo, K. K.-W. *Eur. J. Inorg. Chem.* **2009**, 4265–4273.
(19) Brunner, J.; Barton, J. K. *Biochemistry* **2006**, *45*, 12295–12302.
(20) Yu, M.; Zhao, Q.; Shi, L.; Li, F.; Zhou, Z.; Yang, H.; Yi, T.; Huang, C. *Chem. Commun.* **2008**, 2115–2117.
(21) (a) Lo, K. K.-W.; Lee, P.-K.; Lau, J. S.-Y. *Organometallics* **2008**, *27*, 2998–3006. (b) Lau, J. S.-Y.; Lee, P.-K.; Tsang, K. H.-K.; Ng, C. H.-C.; Lam, Y.-W.; Cheng, S.-H.; Lo, K. K.-W. *Inorg. Chem.* **2009**, *48*, 708–718. (c) Zhang, K. Y.; Lo, K. K.-W. *Inorg. Chem.* **2009**, *48*, 6011–6025.
(22) (a) Lo, K. K.-W.; Chung, C.-K.; Zhu, N. *Chem.—Eur. J.* **2003**, *9*, 475–483. (b) Lo, K. K.-W.; Chung, C.-K.; Lee, T. K.-M.; Lui, L.-H.; Tsang, K. H.-K.; Zhu, N. *Inorg. Chem.* **2003**, *42*, 6886–6897. (c) Lo, K. K.-W.; Chung, C.-K.; Zhu, N. *Chem.—Eur. J.* **2006**, *12*, 1500–1512. (d) Lo, K. K.-W.; Lau, J. S.-Y. *Inorg. Chem.* **2007**, *46*, 700–709. (e) Lo, K. K.-W.; Zhang, K. Y.; Chung, C.-K.; Kwok, K. Y. *Chem.—Eur. J.* **2007**, *13*, 7110–7130. (f) Lo, K. K.-W.; Zhang, K. Y.; Leung, S.-K.; Tang, M. C. *Angew. Chem., Int. Ed.* **2008**, *47*, 2213–2216.
(23) O'Donoghue, K. A.; Kelly, J. M.; Kruger, P. E. *Dalton Trans.* **2004**, 13–15.

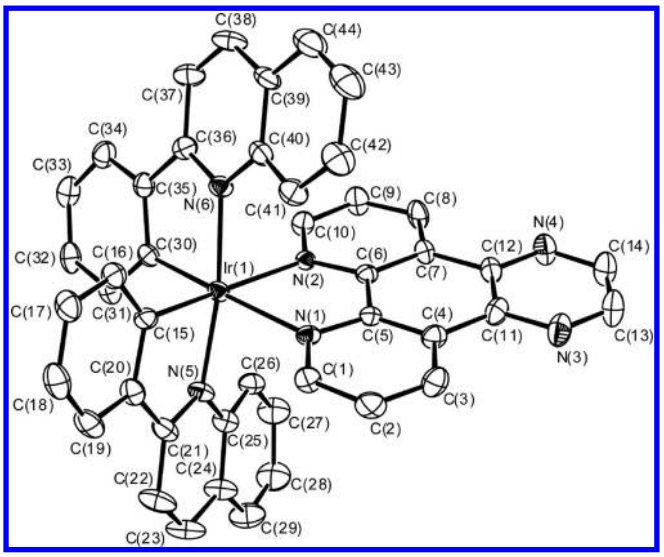

Figure 1. Perspective view of the cation of complex **3a** with the atomic numbering scheme. Thermal ellipsoids are shown at the 20% probability level. Hydrogen atoms are omitted for clarity.

Table 1. Selected Bond Lengths (Å) and Bond Angles (deg) for Complex **3a**

Ir(1)−N(1)	2.191(5)	Ir(1)−N(2)	2.185(5)
Ir(1)−N(5)	2.092(6)	Ir(1)−N(6)	2.099(6)
Ir(1)−C(15)	2.011(7)	Ir(1)−C(30)	1.999(7)
N(1)−Ir(1)−N(2)	75.3(2)	N(1)−Ir(1)−N(5)	84.1(2)
N(1)−Ir(1)−N(6)	102.9(2)	N(1)−Ir(1)−C(15)	95.9(2)
N(1)−Ir(1)−C(30)	171.6(2)	N(2)−Ir(1)−N(5)	105.1(2)
N(2)−Ir(1)−N(6)	81.1(2)	N(2)−Ir(1)−C(15)	169.1(2)
N(2)−Ir(1)−C(30)	97.6(2)	N(5)−Ir(1)−N(6)	171.8(2)
N(5)−Ir(1)−C(15)	80.0(3)	N(5)−Ir(1)−C(30)	93.7(3)
N(6)−Ir(1)−C(15)	94.9(3)	N(6)−Ir(1)−C(30)	80.0(3)
C(15)−Ir(1)−C(30)	91.6(3)		

X-ray Crystal Structure Determination of Complex 3a. The perspective view of the cation of complex **3a** is depicted in Figure 1. Selected bond lengths and bond angles are listed in Table 1. The iridium(III) center of complex **3a** adopted a distorted octahedral geometry and the *trans* angles at the metal center ranged from 169.1(2) to 171.8(2)°. The metal−carbon bonds around the iridium(III) center were in a *cis* orientation. The *trans*-influence of the carbon donors rendered slightly longer Ir−N bond lengths for the dpq ligand (2.185(5) and 2.191(5) Å) than the pq ligands (2.092(6) and 2.099(6) Å). The bite angles of the pq ligands (80.0(3)°) were larger than that of the dpq ligand (75.3(2)°). Similar observations have been made in related cyclometalated iridium(III) polypyridine systems $[Ir(N^{\wedge}C)_2(N^{\wedge}N)]^+$.[22a−c,24]

(24) (a) Neve, F.; Crispini, A.; Campagna, S.; Serroni, S. *Inorg. Chem.* **1999**, *38*, 2250–2258. (b) Neve, F.; La Deda, M.; Crispini, A.; Bellusci, A.; Puntoriero, F.; Campagna, S. *Organometallics* **2004**, *23*, 5856–5863.
(25) King, K. A.; Watts, R. J. *J. Am. Chem. Soc.* **1987**, *109*, 1589–1590.
(26) Didier, P.; Ortmans, I.; Kirsch-De Mesmaeker, A.; Watts, R. J. *Inorg. Chem.* **1993**, *32*, 5239–5245.
(27) Collin, J.-P.; Dixon, I. M.; Sauvage, J.-P.; Williams, J. A. G.; Barigelletti, F.; Flamigni, L. *J. Am. Chem. Soc.* **1999**, *121*, 5009–5016.
(28) (a) Tamayo, A. B.; Alleyne, B. D.; Djurovich, P. I.; Lamansky, S.; Tsyba, I.; Ho, N. N.; Bau, R.; Thompson, M. E. *J. Am. Chem. Soc.* **2003**, *125*, 7377–7387. (b) Sajoto, T.; Djurovich, P. I.; Tamayo, A. B.; Oxgaard, J.; Goddard, W. A., III; Thompson, M. E. *J. Am. Chem. Soc.* **2009**, *131*, 9813–9822. (c) Rausch, A. F.; Thompson, M. E.; Yersin, H. *J. Phys. Chem. A* **2009**, *113*, 5927–5932. (d) Rausch, A. F.; Thompson, M. E.; Yersin, H. *Inorg. Chem.* **2009**, *48*, 1928–1937.

Table 2. Electrochemical Data of the Iridium(III) Dpq and Dpqa Complexes[a]

complex	oxidation, $E_{1/2}$/V	reduction, $E_{1/2}$ or E_c/V
1a	+1.32	−1.29, −1.70,[b] −2.13,[c] −2.31[c]
1b	+1.29	−1.13, −1.67, −2.18,[c] −2.32[c]
2a	+1.14[b]	−1.25, −1.70,[c] −2.01[c]
2b	+1.13[b]	−1.13, −1.64, −2.06[c]
3a	+1.29	−1.27, −1.73,[b] −2.02[c]
3b	+1.30	−1.10, −1.58,[b] −1.95[c]

[a] In CH_3CN (0.1 M $^nBu_4NPF_6$) at 298 K, glassy carbon electrode, sweep rate = 100 mV s^{-1}, all potentials versus SCE. [b] Quasi-reversible waves. [c] Irreversible waves.

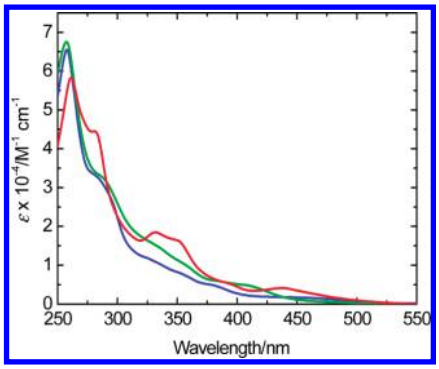

Figure 2. Electronic absorption spectra of complexes **1a** (blue), **2a** (green), and **3a** (red) in CH_2Cl_2 at 298 K.

Electrochemical Properties. The electrochemical properties of all the complexes have been studied by cyclic voltammetry (Table 2). The complexes showed a reversible or quasi-reversible couple at about +1.13 to +1.32 V versus SCE, which has been ascribed to the iridium(IV/III) oxidation.[21,22a−e,24−30] Interestingly, the oxidation couples of the bzq complexes **2a** and **2b** were quasi-reversible and occurred at lower potentials compared to the other complexes, suggesting the possible involvement of σ(Ir−C) bond in this oxidation process.[22b] The first reversible reduction couples of all the complexes have been assigned to the reduction of the diimine ligands.[21,22a−e,24,26,29,30a] This is supported by the fact that the electron-withdrawing amide substituent of the dpqa ligand rendered the first reduction of complexes **1b**−**3b** to occur at less negative potentials (ca. −1.10 to −1.13 V) compared to that of the dpq complexes **1a**−**3a** (ca. −1.25 to −1.29 V) (Table 2). The reduction waves at more negative potentials are quasi-reversible or highly irreversible and have been assigned to the reduction of the diimine and the cyclometalating ligands.[21,22a−e,24,26,29]

Electronic Absorption and Luminescence Properties. The electronic absorption spectral data of all the complexes in CH_2Cl_2 and CH_3CN at 298 K are listed in Supporting Information, Table S1. The electronic absorption spectra of complexes **1a**−**3a** in CH_2Cl_2 at 298 K are shown in Figure 2. With reference to related iridium(III) complexes, the intense absorption bands and shoulders at 255−332 nm have been assigned to spin-allowed intraligand (^{1}IL)

(29) Avilov, I.; Minoofar, P.; Cornil, J.; De Cola, L. *J. Am. Chem. Soc.* **2007**, *129*, 8247–8258.
(30) (a) Liu, S.-J.; Zhao, Q.; Chen, R.-F.; Deng, Y.; Fan, Q.-L.; Li, F.-Y.; Wang, L.-H.; Huang, C.-H.; Huang, W. *Chem.—Eur. J.* **2006**, *12*, 4351–4361. (b) Li, X.; Chen, Z.; Zhao, Q.; Shen, L.; Li, F.; Yi, T.; Cao, Y.; Huang, C. *Inorg. Chem.* **2007**, *46*, 5518–5527.

Table 3. Photophysical Data of the Iridium(III) Dpq and Dpqa Complexes

complex	medium (T/K)	λ_{em}/nm	τ_o/μs	Φ_{em}
1a	MeOH (298)	577	0.20	0.066
	CH_3CN (298)	576	0.35	0.11
	CH_2Cl_2 (298)	566	0.75	0.34
	Glass[a] (77)	503, 538 sh	5.27	
1b	MeOH (298)	597	0.65 (22%), 0.11 (78%)	0.00016
	CH_3CN (298)	589	0.047	0.012
	CH_2Cl_2 (298)	572	0.59	0.31
	Glass[a] (77)	506, 545 sh	4.17	
2a	MeOH (298)	596	0.15	0.031
	CH_3CN (298)	600	0.26	0.10
	CH_2Cl_2 (298)	590	0.56	0.30
	Glass[a] (77)	498 sh, 533	50.3 (32%), 5.90 (68%)	
2b	MeOH (298)	586	0.58 (36%), 0.16 (64%)	0.00048
	CH_3CN (298)	606	0.028	0.013
	CH_2Cl_2 (298)	601	0.37	0.13
	Glass[a] (77)	496 sh, 529	52.1 (27%), 3.19 (73%)	
3a	MeOH (298)	558, 604 sh	0.71	0.12
	CH_3CN (298)	557, 601 sh	1.24	0.40
	CH_2Cl_2 (298)	555, 598 sh	1.54	0.47
	Glass[a] (77)	540 (max), 582, 623 sh	4.67	
3b	MeOH (298)	574	7.07 (24%), 0.82 (76%)	0.0010
	CH_3CN (298)	564, 594 sh	0.22	0.031
	CH_2Cl_2 (298)	578	0.91	0.18
	Glass[a] (77)	540 (max), 584, 627 sh	4.69	

[a] EtOH/MeOH (4:1, v/v).

($\pi \rightarrow \pi^*$) (N^N and N^C) transitions.[21,22a−e,24,26−28,30] The less intense absorption bands and shoulders at >340 nm and the weak absorption tailing at 450−550 nm have been assigned to spin-allowed[21,22a−e,24,26−28,30] and spin-forbidden [21,22a−e,24,27,28,30] metal-to-ligand charge-transfer (MLCT) (dπ(Ir) → π^*(N^N and N^C)) transitions, respectively.

Upon photoexcitation, all the complexes exhibited intense and long-lived green to orange luminescence in relatively nonpolar organic solutions under ambient conditions and in low-temperature glass. The photophysical data of all the complexes are summarized in Table 3. The emission spectra of complexes **1a** and **3a** in CH_2Cl_2 at 298 K and in alcohol glass at 77 K are shown in Figure 3. Complexes **1a**, **1b**, **2a**, and **2b** showed highly environment-sensitive emission; for example, upon changing the solvent from MeOH to less polar CH_2Cl_2, the complexes showed higher quantum yields and longer emission lifetimes. This indicates that the emission originated from a ^{3}MLCT (dπ(Ir) → π^*(N^N)) emissive state.[21,22,24−26,28,29,30b] Interestingly, the increase of the emission quantum yields on going from MeOH to CH_2Cl_2 is much more significant for the dpqa complexes **1b** and **2b** compared to the dpq complexes **1a** and **2a**. We ascribe this to the hydrogen-bonding interactions between the amide group of the dpqa ligand and protic solvent molecules.[22c] Complex **3a** exhibited structured emission spectra in fluid solutions at 298 K (Figure 3), and its emission quantum yield was less sensitive to the polarity of the solvents (Table 3), indicative of an emissive state of substantial ^{3}IL ($\pi \rightarrow \pi^*$) (pq) character.[21a,b,22b,e] On the contrary, the pq−dpqa complex **3b** did not display rich structural features; its emission quantum yield showed strong dependence on the polarity of solvents; and its emission lifetimes were noticeably shorter than those of other iridium(III)-pq complexes. Thus, the emissive state of this complex should possess predominant ^{3}MLCT (dπ(Ir) → π^*(dpqa)) character.[22e] The dpqa complexes **1b**−**3b** showed biexponential decay in MeOH, which has been tentatively assigned to ^{3}MLCT (dπ(Ir) → π^*(dpqa)) and ^{3}MLCT (dπ(Ir) → π^*(N^C)) excited states, respectively. Upon cooling to 77 K, the emission maxima of complexes **1a**, **2a**, **1b**, and **2b** showed significant blue shifts (Table 3 and Figure 3), pointing to an excited state of ^{3}MLCT (dπ(Ir) → π^*(N^N)) character.[21,22,24−26,28,29,30b] Both complexes **2a** and **2b** showed biexponential decay with lifetimes of about 50−52 and 3.2−5.9 μs, which are possibly associated with ^{3}MLCT (dπ(Ir) → π^*(bzq)) and ^{3}MLCT (dπ(Ir) → π^*(N^N)) states, respectively.[22b,d,26] The pq complexes **3a** and **3b** showed a highly structured emission band and a much smaller blue shift upon cooling to 77 K (Table 3 and Figure 3). It is conceivable that the emission is derived

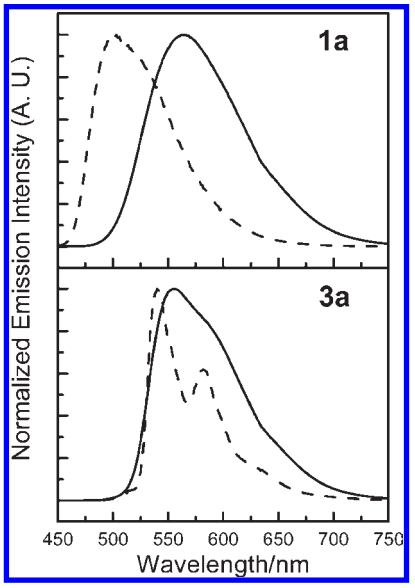

Figure 3. Emission spectra of complexes **1a** and **3a** in CH_2Cl_2 (solid) at 298 K and in EtOH/MeOH (4:1, v/v) at 77 K (dashed).

Table 4. Lipophilicity and Cytotoxicity (IC_{50}, 48 h) of the Iridium(III) Dpq and Dpqa Complexes and Cisplatin Toward the HeLa and MDCK Cell Lines

complex	lipophilicity	IC_{50}(HeLa)/μM	IC_{50}(MDCK)/μM
1a	0.90	6.2 ± 0.6	15.3 ± 3.4
1b	1.83	10.8 ± 1.4	25.2 ± 3.9
2a	2.98	2.7 ± 0.2	4.6 ± 0.4
2b	3.38	3.3 ± 0.4	8.0 ± 1.0
3a	2.82	1.3 ± 0.1	4.0 ± 0.3
3b	3.95	2.0 ± 0.1	7.4 ± 1.0
cisplatin	-2.30[a]	26.1 ± 4.1	36.6 ± 6.5

[a] From reference 33.

from a ^{3}IL ($\pi \rightarrow \pi^*$) (pq) state that may be mixed with some ^{3}CT character.[21a,b,22b,e]

Lipophilicity and Cytotoxicity. The ability of a cellular probe to permeate biological membranes depends strongly on its lipophilicity,[31] which is commonly estimated by the partition coefficient of the compound in *n*-octanol/water ($P_{o/w}$).[32] The lipophilicity (log $P_{o/w}$ values) of the iridium(III) dpq and dpqa complexes in this work has been determined (Table 4). The lipophilicity of all the iridium(III) dpq and dpqa complexes (from 0.90 to 3.95) is significantly higher than that of cisplatin (-2.30)[33] and comparable to or higher than that of ruthenium(II) dipyridophenazine complexes (ca. -2.50 to 1.30),[11a] which is due to the lower cationic charge of the iridium(III) complexes. The bzq and pq complexes showed substantially higher lipophilicity than the ppz complexes, which is in accordance with the hydrophobic nature of the cyclometalating ligands. Additionally, the lipophilicity of the dpqa complexes is higher than that of the dpq complexes, possibly because of the *n*-butyl chain.

The cytotoxicity of all the complexes toward the HeLa and MDCK cell lines has been studied by the 3-(4,5-dimethyl-2-thiazolyl)-2,5-diphenyltetrazolium bromide (MTT) assay,[34] in which the dose dependence of surviving cells after exposure to the complexes for 48 h has been evaluated. The IC_{50} values of all the complexes (Table 4) range from 1.3 to 10.8 μM toward HeLa cells, which are lower than that of cisplatin (26.1 μM) under the same experimental conditions. These IC_{50} values are also smaller than those of $[Re(CO)_3(2\text{-appt})Cl]$ (2-appt = 2-amino-4-phenylamino-6-(2-pyridyl)-1,3,5-triazine) (IC_{50} = 50 μM) and $[Ru(^tBu_2\text{-bpy})_2(2\text{-appt})]^{2+}$ ($^tBu_2$-bpy = 4,4′-di-*tert*-butyl-2,2′-bipyridine) (IC_{50} = 59.7 μM), both of which bind to the minor groove of double-stranded DNA.[35] Similar cytotoxicity toward HeLa cells has been reported for other cyclometalated iridium(III) polypyridine complexes (IC_{50} = 1.1 to 18.1 μM).[21] In this work, the IC_{50} values of all the complexes toward MDCK cells in a 48 h incubation period are larger (4.0 to 25.2 μM) (Table 4). In general, the higher cytotoxicity of the bzq and pq complexes compared to that of the ppz complexes is likely to be a consequence of their higher lipophilicity.[21a,c]

Cellular Uptake and Localization Studies. The cellular uptake properties of these complexes have been investigated using laser-scanning confocal microscopy. Treatment of HeLa cells with the complexes resulted in rapid and extensive cell death, most likely because of the high cytotoxicity of the complexes. Thus, MDCK cells have been used as a model in our imaging study. The plasma membrane of MDCK cells remained impermeable to propidium iodide after treatment with the complexes (50 μM) in an incubation period of 3 h, suggesting that the cells were viable during the imaging experiments. The microscopy images of MDCK cells treated with complex **3a** are illustrated in Figure 4. MDCK cells incubated with the complex for 1 h showed cytoplasmic staining. As the incubation proceeded, the cells revealed increasing emission intensities, indicating that more complex molecules penetrated the plasma membrane and entered the cells. Importantly, after 90 min, the complex was detectable in the nucleus; after 120 min, staining of nuclear structures reminiscent of the nucleoli was clearly observed (Figure 4). Other complexes also gave similar staining results (Figure 5). The cytoplasm and the nucleolus of the cells displayed very strong emission while the nucleoplasm emitted weakly. Although cellular internalization of luminescent cyclometalated iridium(III) polypyridine complexes has been reported,[20,21] the observations of nuclear uptake and nucleolar staining are unprecedented.[36] It is important to point out that although the nuclear uptake properties of ruthenium(II)- and rhodium(III)-octaarginine-fluorophore conjugates have been reported,[11c,19] the incorporated oligopeptide and/or the fluorescein moieties of these complexes play a critical role in the uptake process. To the best of our knowledge, the iridium(III) complexes in this work are very rare luminescent transition metal complexes that show nucleoli-staining capability.[15b] We believe that the efficient cellular and nuclear uptake of these iridium(III) complexes is due to their low cationic charge and high lipophilicity,[17] and the use of the dpq and dpqa ligands which allow the complexes to be retained inside the nucleus because of their binding to the nucleoli, nucleic acids, and possibly intranuclear proteins (see below). Interestingly, MDCK cells fixed with MeOH before treatment with the complexes revealed similar staining in both the cytoplasm and the nucleolus (Figure 6). This reflects that the observed intracellular distribution of these complexes was due to their affinity to cellular structures, rather than a consequence of active sequestration by the living cells. To confirm the intranuclear structures labeled by the complexes were indeed nucleoli, we co-stained fixed MDCK cells with complex **1a** (5 μM, 1 h) and an antibody against nucleolar protein fibrillarin (20 μL/mL, 1 h), using Alexa-633 antirabbit IgG (20 μg/mL, 30 min) as the secondary antibody. As shown in Figure 7, the intranuclear staining of complex **1a** colocalized with fibrillarin. After treatment with ribonuclease A (50 μg/mL, 1 h, 37 °C), fixed MDCK cells loaded with the

(31) VanBrocklin, H. F.; Liu, A.; Welch, M. J.; O'Neil, J. P.; Katzenellenbogen, J. A. *Steroids* **1994**, *59*, 34–45.
(32) Minick, D. J.; Frenz, J. H.; Patrick, M. A.; Brent, D. A. *J. Med. Chem.* **1988**, *31*, 1923–1933.
(33) Oldfield, S. P.; Hall, M. D.; Platts, J. A. *J. Med. Chem.* **2007**, *50*, 5227–5237.
(34) Mosmann, T. *J. Immunol. Methods* **1983**, *65*, 55–63.
(35) Ma, D.-L.; Che, C.-M.; Siu, F.-M.; Yang, M.; Wong, K.-Y. *Inorg. Chem.* **2007**, *46*, 740–749.
(36) Interestingly, luminescent lanthanide chelates have been designed as nucleolar staining agents. See, for example, (a) Yu, J.; Parker, D.; Pal, R.; Poole, R. A.; Cann, M. J. *J. Am. Chem. Soc.* **2006**, *128*, 2294–2299. (b) Pal, R.; Parker, D. *Chem. Commun.* **2007**, 474–476. (c) Pal, R.; Parker, D. *Org. Biomol. Chem.* **2008**, *6*, 1020–1033.

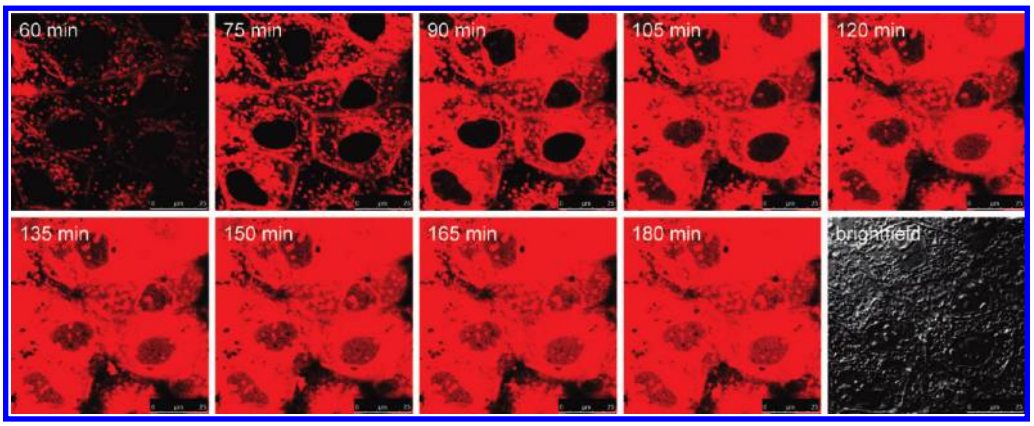

Figure 4. Time lapse laser-scanning confocal microscopy images of MDCK cells incubated with complex **3a** (50 μM) for 1 h over another 2 h at 37 °C. The brightfield image was taken after incubation for 3 h.

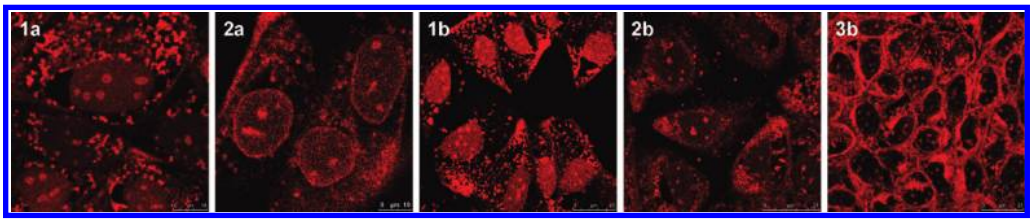

Figure 5. Fluorescence laser-scanning confocal microscopy images of MDCK cells treated with complexes **1a**, **2a**, and **1b**−**3b** (50 μM) at 37 °C for 3 h.

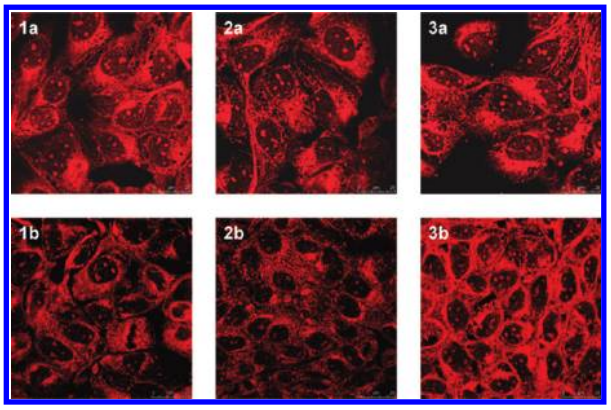

Figure 6. Fluorescence laser-scanning confocal microscopy images of fixed MDCK cells treated with the iridium(III) dpq and dpqa complexes (5 μM) at room temperature for 30 min.

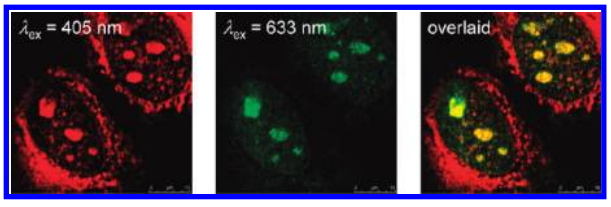

Figure 7. Fluorescence laser-scanning confocal microscopy images of fixed MDCK cells treated successively with fibrillarin antibody (20 μL/mL, 1 h), Alexa 633 antirabbit IgG antibody (20 μg/mL, 30 min), and complex **1a** (5 μM, 30 min).

complexes still showed nucleolar staining (Figure 8), suggesting that the emission observed in the microscopy studies did not originate from interactions of the complexes with RNA.

Binding to Biomolecules. As the nucleolus is composed of proteins and nucleic acids, the possible interactions of these iridium(III) dpq and dpqa complexes with proteins, DNA, and RNA have been investigated by emission titrations and SDS-PAGE gel staining. First, the interactions of these complexes with a model protein bovine serum albumin (BSA) have been studied by emission titrations.[37] In aqueous buffer solution, the dpq complexes emitted very weakly, and the dpqa complexes were not emissive because of the hydrogen-bonding interactions between the quinoxaline nitrogen atoms of the complexes (and the amide moiety of the dpqa complexes) and water molecules. Upon addition of BSA, however, the emission intensities of the dpq complexes were significantly increased, and the dpqa complexes displayed new emission bands. At [BSA] = 1 mM, the complexes ([Ir] = 10 μM) revealed about 11.71- to 76.25-fold increase in emission intensities (Table 5). The emission spectral traces and titration curve of complex **3b** upon addition of BSA are shown in Figure 9. These changes of photophysical properties have been ascribed to the binding of the complexes to hydrophobic pockets of the

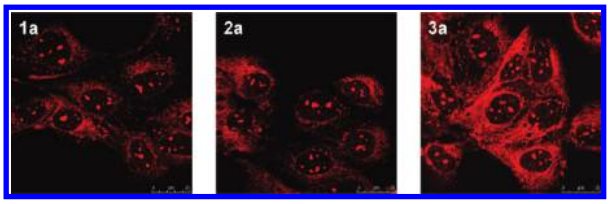

Figure 8. Fluorescence laser-scanning confocal microscopy images of fixed MDCK cells treated successively with ribonuclease A (50 μg/mL, 1 h, 37 °C) and complexes **1a**−**3a** (5 μM, 30 min).

(37) Binding of transition metal dpq complexes to serum albumins has been reported. See, for example, (a) Maity, B.; Roy, M.; Saha, S.; Chakravarty, A. R. *Organometallics* **2009**, *28*, 1495–1505. (b) Saha, S.; Majumdar, R.; Roy, M.; Dighe, R. R.; Chakravarty, A. R. *Inorg. Chem.* **2009**, *48*, 2652–2663.

Table 5. Photophysical Properties of the Iridium(III) Dpq and Dpqa Complexes (10 μM) in the Absence and Presence of BSA (50 μM), Ds-CT-DNA (0.45 mM), and Torula Yeast RNA (0.45 mM) at 298 K

complex	biomolecule	λ_{em}/nm	τ_o/μs	I^a
1a	buffer only[b]	596	0.47 (10%), 0.089 (90%)	1.00
	BSA[b]	571	0.58 (42%), 0.17 (58%)	11.71
	DNA[c]	574	0.31 (50%), 0.16 (50%)	27.12
	RNA[c]	596	0.55 (13%), 0.099 (87%)	1.04
1b[d,e,f]	BSA[b]	587	0.44 (39%), 0.14 (61%)	21.70
2a	buffer only[b]	592	0.51 (33%), 0.13 (67%)	1.00
	BSA[b]	568	0.69 (33%), 0.23 (67%)	29.36
	DNA[c]	597	0.40 (29%), 0.12 (71%)	37.64
	RNA[c]	592	0.40 (31%), 0.10 (69%)	1.20
2b[d,f]	BSA[b]	578	0.88 (22%), 0.17 (78%)	52.70
	DNA[c]	592	0.19 (29%), 0.062 (71%)	8.52
3a	buffer only[b]	560, 604 sh	0.76 (35%), 0.29 (65%)	1.00
	BSA[b]	560, 605 sh	1.85 (46%), 0.70 (54%)	28.82
	DNA[c]	560, 597 sh	0.89 (53%), 0.31 (47%)	18.53
	RNA[c]	560, 600 sh	1.08 (23%), 0.34 (77%)	1.16
3b[d,e,f]	BSA[b]	560, 600 sh	1.39 (31%), 0.34 (69%)	76.25

[a] Relative emission intensities of the complexes (10 μM). [b] Potassium phosphate buffer (50 mM, pH 7.4)/MeOH (7:3, v/v). [c] Tris-Cl buffer (50 mM, pH 7.4)/MeOH (7:3, v/v). [d] The emission of the free complex was too weak for accurate measurements. [e] The emission of the complex in the presence of DNA was too weak for accurate measurements. [f] The emission of the complex in the presence of RNA was too weak for accurate measurements.

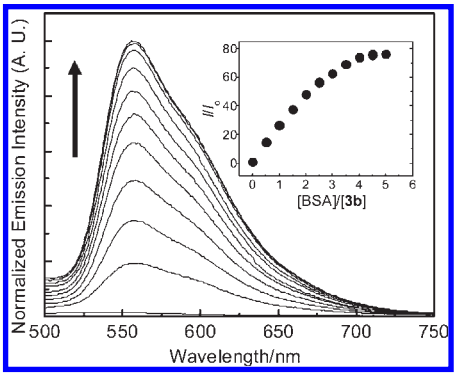

Figure 9. Emission spectral traces of complex **3b** (10 μM) in potassium phosphate buffer (50 mM, pH 7.4)/MeOH (7:3, v/v) at 298 K in the presence of BSA (0−50 μM). The inset shows the emission titration curve (emission intensity monitored at 560 nm).

protein. This is supported by the facts that upon addition of BSA, the emission maxima of the ^{3}MLCT emitter complexes **1a** and **2a** were blue-shifted from 596 to 571 nm and from 592 to 568 nm, respectively, and the emission lifetimes were also increased (Table 5), indicative of the more hydrophobic local surroundings of the complexes. The binding constants ($K_{a,BSA}$) of these complexes to BSA ranged from 4.9×10^4 to 1.1×10^5 M^{-1} (Table 6), which are similar to those of related iridium(III) indole complexes ($K_a = 3.1 \times 10^4$ to 6.3×10^4 M^{-1}),[21b] a copper(II) dpq complex ($K_a = 1.2 \times 10^5$ M^{-1}),[37a] and an iron(III) dpq complex ($K_a = 1.3 \times 10^5$ M^{-1}).[37b] The Hill coefficients (n_H) were all >1 (Table 6), indicative of cooperative binding. Since binding of the complexes to BSA resulted in significant emission enhancement, we have studied the possible staining of proteins in polyacrylamide gel with the complexes. An SDS-PAGE gel containing proteins from various tissues of Medaka and subcellular fractions of Human Umbilical Vein Endothelial Cells (HUVEC) and a 2D SDS-PAGE gel containing total proteins from MDCK cells, after staining with

Table 6. Parameters for the Binding of the Iridium(III) Dpq and Dpqa Complexes to BSA and Ds-CT-DNA at 298 K

complex	$K_{a,BSA}$/M^{-1}	n_H[a]	$K_{a,DNA}$/M^{-1}
1a	4.9×10^4	1.6	6.8×10^4
1b	6.4×10^4	2.0	b
2a	7.1×10^4	2.2	3.7×10^4
2b	7.8×10^4	1.8	5.2×10^3
3a	1.1×10^5	2.3	4.8×10^4
3b	7.9×10^4	2.1	b

[a] n_H is the Hill coefficient for BSA-binding. [b] Not determined because of no observable changes.

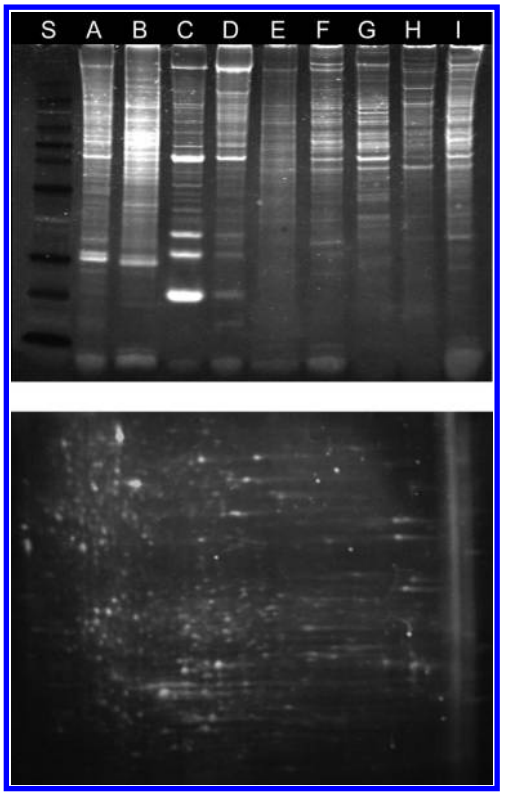

Figure 10. Top: SDS-PAGE analysis of proteins upon staining with complex **3a** under ultraviolet transillumination. Lanes A−D correspond to the proteins form the gill, liver, muscle, and skin of Medaka, respectively. Lane E corresponds to total proteins of HUVEC. Lanes F−I correspond to proteins from the cytoplasm, nucleus, nucleoplasm, and nucleolus of HUVEC, respectively. Lane S corresponds to protein markers. Bottom: 2D SDS-PAGE analysis of total proteins from MDCK cells upon staining with complex **3a** under ultraviolet transillumination.

complex **3a** (50 μM, 30 min), are shown in Figure 10. Both gels were brightly stained and similar results were obtained by Coomassie Blue staining, indicative of the general binding of complex **3a** to various proteins in these cells.

The interactions of these complexes with double-stranded calf thymus DNA (ds-CT-DNA) have also been investigated by emission titrations. The dpq complexes **1a**−**3a** displayed significant emission enhancement (ca. 18.5- to 37.6-fold) in the presence of ds-CT-DNA (Table 5, Figure 11). The titration curve of complex **2a** is shown in Figure 12. The emission enhancement has been ascribed to the intercalation of the complexes into the base-pairs of the ds-CT-DNA molecules, resulting in increased hydrophobicity and rigidity of the local surroundings of the complexes and the protection of the dpq ligands from interacting with the water molecules.

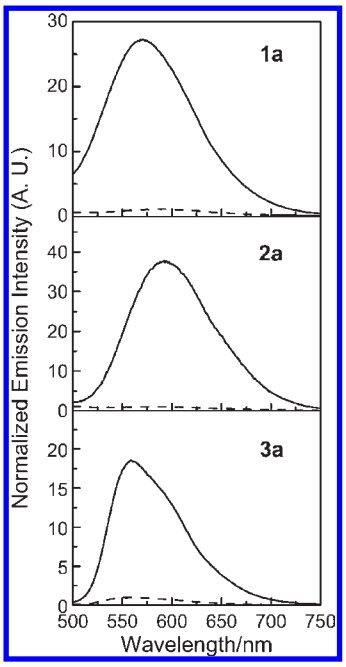

Figure 11. Emission spectra of complexes **1a**−**3a** (10 μM) in Tris-Cl buffer (50 mM, pH 7.4)/MeOH (7:3, v/v) in the absence (dashed) and presence (solid) of ds-CT-DNA (0.45 mM).

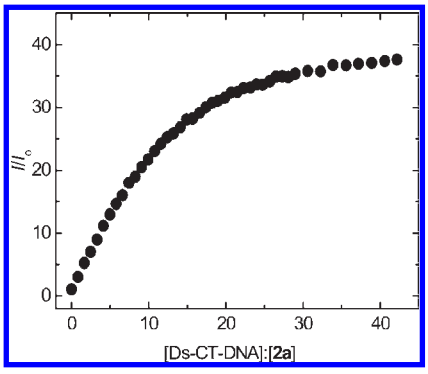

Figure 12. Emission titration curve for the titration of complex **2a** (10 μM) with ds-CT-DNA. The emission intensity of complex was monitored at 597 nm.

The intrinsic binding constants ($K_{a,DNA}$) were determined to be about 3.7×10^4 to 6.8×10^4 M^{-1} for the binding of the dpq complexes to ds-CT-DNA (Table 6), which are comparable to those observed for $[Ru(bpy)_2(dpq)]^{2+}$ (bpy = 2,2′-bipyridine) ($K_a = 5.9 \times 10^4$ M^{-1})[38a] and $[Ir(ppy)_2(dpq)]^+$ (Hppy = 2-phenylpyridine) ($K_a = 1.2 \times 10^4$ M^{-1}).[22c] Remarkably, we found that both the dpqa complexes **1b** and **3b** did not show any change in their emission properties although their ppy counterpart $[Ir(ppy)_2(dpqa)]^+$ exhibited 40-fold emission enhancement upon binding to ds-CT-DNA ($K_a = 1.1 \times 10^4$ M^{-1}).[22c] It is unlikely that the *n*-butylamide moiety of the dpqa ligand would hamper the DNA-intercalating properties of these two complexes because both $[Ir(ppy)_2(dpqa)]^+$[22c] and $[Ru(bpy)_2(dpqa)]^{2+}$[23] are DNA-intercalators with binding affinities comparable to those of their respective dpq counterparts. The lack of emission enhancement could be due to an effective nonradiative deactivation pathway for the iridium-DNA adducts. In contrast, a new emission band was observed for complex **2b** upon addition of ds-CT-DNA, and the intensity was about 8.52 times the background when DNA was absent (Table 5). The binding constant was determined to be 5.2×10^3 M^{-1}, which is one order of magnitude smaller than those for the dpq complexes (3.7×10^4 to 6.8×10^4 M^{-1}) (Table 6). Since the dpq and dpqa complexes should bind to ds-CT-DNA with similar affinities (see above), the weaker binding of complex **2b** may be due to the possibility that it binds via intercalation of its bzq ligands. It is interesting to note that the binding constant of this complex is similar to that of $[Ru(phen)_2(bpy)]^{2+}$ (2.4×10^3 M^{-1}),[38b] which intercalates into DNA with its phen ligands. Emission titrations showed that the photophysical properties of all the complexes in aqueous buffer did not change significantly upon addition of torula yeast RNA (Table 5), suggestive of the absence of interactions. This is not unexpected since most luminescent transition metal-based intercalators respond to ds-DNA instead of RNA.[22c,23,38] Also, this is in agreement with the confocal microscopy studies which showed that fixed MDCK cells treated with ribonuclease A still showed nucleolar staining by the complexes (Figure 8).

Taken together, all these results show that the iridium(III) complexes were permeable to living mammalian cells and could accumulate in the cytoplasm and nucleolus, possibly through binding to hydrophobic pockets of proteins and intercalating into ds-DNA. Since these complexes were nearly non-emissive in aqueous medium, it is very likely that the emission observed in the stained cells originated from protein- and/or DNA-bound complexes. Intriguingly, despite the relatively strong DNA-induced emission properties of these complexes, the nucleoplasm was largely unstained whereas the nucleolus was strongly labeled. On the basis of the results from the protein titrations and gel staining experiments, it is reasonable to assume that the emission of the nucleoli was due to protein-bound complexes. Although bioinformatic analysis of the amino acid usage of nucleolar proteins does not reveal preference to hydrophobic amino acids,[39] previous cell biology work using 8-anilino-l-naphthalene-sulfonate shows distinct nucleolar staining by this hydrophobic probe.[40,41] Also, the lipophilic dye Nile Red can label the nucleolus in addition to the expected oil droplet staining.[42] These observations indicate that the nucleolus can be imaged using hydrophobic probes with low cationic charge, high lipophilicity, and strong environment-sensitive emission properties such as the cyclometalated iridium(III) dipyridoquinoxaline complexes in this work. We anticipate that these findings will form a basis for further development of nucleolar markers.

Conclusions

In summary, a series of luminescent cyclometalated iridium(III) dipyridoquinoxaline complexes has been synthesized and characterized, and their photophysical and

(38) (a) Delaney, S.; Pascaly, M.; Bhattacharya, P. K.; Han, K.; Barton, J. K. *Inorg. Chem.* **2002**, *41*, 1966–1974. (b) Pyle, A. M.; Rehmann, J. P.; Meshoyrer, R.; Kumar, C. V.; Turro, N. J.; Barton, J. K. *J. Am. Chem. Soc.* **1989**, *111*, 3051–3058.

(39) Leung, A. K. L.; Andersen, J. S.; Mann, M.; Lamond, A. I. *Biochem. J.* **2003**, *376*, 553–569.

(40) Dyckman, J.; Weltman, J. K. *J. Cell. Biol.* **1970**, *45*, 192–197.

(41) Cowden, R. R.; Curtis, S. K. *Histochem. J.* **1974**, *6*, 447–450.

(42) Diaz, G.; Melis, M.; Batetta, B.; Angius, F.; Falchi, A. M. *Micron* **2008**, *39*, 819–824.

electrochemical properties investigated. The lipophilicity, cytotoxicity, and cellular uptake properties of all the complexes have been examined. The IC_{50} values of the complexes toward HeLa and MDCK cell lines ranged from about 1.1 to 10.8 and 4.0 to 25.2 μM, respectively. Treatment of MDCK cells with the complexes resulted in significant nucleolar staining. Emission titrations and gel staining experiments revealed that the complexes bound to hydrophobic pockets of proteins, intercalated into ds-CT-DNA, but did not interact with RNA. These complexes, to the best of our knowledge, are the first examples of luminescent iridium(III) polypyridines that show nuclear uptake and nucleolar staining in live cells. Studies of related luminescent transition metal complexes are underway.

Experimental Section

General Comments and Instrumentation. All solvents were of analytical reagent grade and purified according to standard procedures.[43] All buffer components were of biological grade and used as received. $IrCl_3 \cdot 3H_2O$, Hppz, Hbzq, Hpq, *n*-octanol, 4-methoxyaniline, 4-methoxyphenol, phenol, acetophenone, naphthalene, *t*-butylbenzene, anthracene, and pyrene were purchased from Aldrich. KPF_6 and cisplatin were purchased from Acros. MTT and HUVEC culture medium were purchased from Sigma. Ds-CT-DNA and BSA were obtained from Calbiochem. Ds-CT-DNA was purified by phenol extraction as described[44] and the concentration per base-pair was determined from absorption spectroscopy ($\varepsilon_{260\ nm}$ = 6,600 M^{-1} cm^{-1}). Dpq,[45] dpqa,[46] and the precursor iridium dimer complexes $[Ir_2(N^{\wedge}C)_4Cl_2]$[47] were prepared according to reported procedures. Tetra-*n*-butylammonium hexafluorophosphate was obtained from Aldrich and was recrystallized from hot ethanol and dried in vacuo at 110 °C before use. HeLa, MDCK, and HUVEC cells were obtained from American Type Culture Collection. Three-month old marine Medaka (Oryzias javanicus) were obtained from the fish stock of the Research Center of Coastal Pollution and Conservation, City University of Hong Kong. Dulbecco's modified Eagle's medium (DMEM), fetal bovine serum (FBS), phosphate buffered saline (PBS), trypsin-EDTA, penicillin/streptomycin, propidium iodide, fibrillarin antibody, Alexa-633 antirabbit IgG antibody, ribonuclease A, SDS-sample buffer, and Novex precast gel were purchased from Invitrogen. The 2D gel sample buffer and Ettan 2D gel apparatus were purchased from GE Healthcare. The growth medium for cell culture contained DMEM with 10% FBS and 1% penicillin/streptomycin. The instrumentation for physical measurements has been described previously.[21c] Electronic absorption, steady-state emission spectra were recorded on a Hewlett-Packard 8453 diode array spectrophotometer and a SPEX FluoroLog 3-TCSPC spectrophotometer, respectively. Emission lifetimes were measured in the Fast MCS mode with a NanoLED N-375 as the excitation source. Unless specified, all the solutions for photophysical studies were degassed with no fewer than four successive freeze−pump−thaw cycles and stored in a 10 cm^3 round-bottomed flask equipped with a side arm 1 cm fluorescence cuvette and sealed from the atmosphere by a Rotaflo HP6/6 quick-release Teflon stopper. Luminescence quantum yields were measured by the optically dilute method[48] with an aerated aqueous solution of $[Ru(bpy)_3]Cl_2$ (Φ_{em} = 0.028, λ_{ex} = 455 nm)[49] as the standard solution. The electrochemical measurements were performed on a CH Instruments Electrochemical Workstation CHI750A. Cyclic voltammetry experiments were carried out at room temperature using a two-compartment glass cell with a working volume of 500 μL. A platinum gauze counter electrode was accommodated in the working electrode compartment. The working and reference electrodes were a glassy carbon electrode and a $Ag/AgNO_3$ (0.1 M $^nBu_4NPF_6$ in CH_3CN) electrode, respectively. The reference electrode compartment was connected to the working electrode compartment via a Luggin capillary. Solutions for electrochemical measurements were degassed with prepurified argon gas. Ferrocene was used as an internal standard and all potentials were referred to SCE.

Synthesis of $[Ir(N^{\wedge}C)_2(N^{\wedge}N)](PF_6)$. A mixture of $[Ir_2(N^{\wedge}C)_4Cl_2]$ (0.10 mmol) and dpq or dpqa (0.20 mmol) in $MeOH/CH_2Cl_2$ (30 mL, 1:1, v/v) was refluxed under an inert atmosphere of nitrogen in the dark for 4 h. The yellow solution was then cooled to room temperature, and KPF_6 (0.22 mmol) was added to the solution. The mixture was then evaporated to dryness. The solid was dissolved in CH_2Cl_2 and purified by column chromatography on silica gel. The desired product was eluted with CH_2Cl_2/acetone (1:1, v/v) and recrystallized from acetone/diethyl ether.

$[Ir(ppz)_2(dpq)](PF_6)$ (1a). Complex **1a** was isolated as yellow crystals. Yield: 122 mg (71%). ^1H NMR (300 MHz, acetone-d_6, 298 K, TMS): δ = 9.78 (dd, J = 8.2, 1.4 Hz, 2H; H4, H4′ pyrido rings dpq), 9.35 (s, 2H; H2, H3 quinoxaline dpq), 8.72 (d, J = 2.9 Hz, 2H; H5, pyrazole ring ppz), 8.69 (dd, J = 5.0, 1.5 Hz, 2H; H6, H6′ pyrido rings dpq), 8.23 (dd, J = 8.2, 5.2 Hz, 2H; H5, H5′ pyrido ring dpq), 7.68 (d, J = 8.2 Hz, 2H; H3 phenyl ring ppz), 7.24 (d, J = 2.1 Hz, 2H; H3 pyrazole ring ppz), 7.11 (dt, J = 7.6, 1.5 Hz, 2H; H4 phenyl ring ppz), 6.93 (dt, J = 7.6, 1.2 Hz, 2H; H5 phenyl ring ppz), 6.61 (t, J = 2.3 Hz, 2H; H4 pyrazole ring ppz), 6.45 (dd, J = 7.3, 1.2 Hz, 2H; H6 phenyl ring ppz). IR (KBr) ν/cm^{-1}: 842 (PF_6^-). Positive-ion ESI-MS ion cluster at m/z 711 $\{M - PF_6^-\}^+$. Anal. Calcd for $C_{32}H_{22}F_6IrN_8P$: C, 44.91; H, 2.61; N, 13.09. Found: C, 44.91; H, 2.90; N, 13.21.

$[Ir(ppz)_2(dpqa)](PF_6)$ (1b). Complex **1b** was isolated as yellow crystals. Yield: 138 mg (72%). ^1H NMR (300 MHz, acetone-d_6, 298 K, TMS): δ = 10.28 (dd, J = 8.4, 1.5 Hz, 1H; H4 pyrido ring dpqa), 9.85 (s, 1H; H3 quinoxaline dpqa), 9.81 (dd, J = 8.1, 1.5 Hz, 1H; H4′ pyrido ring dpqa), 9.16 (t, J = 6.5 Hz, 1H; NH), 8.73−8.69 (m, 4H; H6, H6′ pyrido rings dpq, H5 pyrazole ring ppz), 8.28−8.20 (m, 2H; H5, H5′ pyrido rings dpq), 7.68 (d, J = 7.8 Hz, 2H; H3 phenyl ring ppz), 7.27 (d, J = 2.4 Hz, 1H; H3 pyrazole ring ppz), 7.21 (d, J = 2.1 Hz, 1H; H3 pyrazole ring ppz), 7.11 (dt, J = 7.8, 1.2 Hz, 2H; H4 phenyl ring ppz), 6.93 (t, J = 7.2 Hz, 2H; H5 phenyl ring ppz), 6.61 (q, J = 3.0 Hz, 2H; H4 pyrazole ring ppz), 6.45 (d, J = 7.5 Hz, 2H; H6 phenyl ring ppz), 3.56 (q, J = 7.5 Hz, 2H; $CH_2CH_2CH_2CH_3$), 1.67 (quin, J = 7.5 Hz, 2H; $CH_2CH_2CH_2CH_3$), 1.44 (sext, J = 7.5 Hz, 2H; $CH_2CH_2CH_2CH_3$), 0.95 ppm (t, J = 7.5 Hz, 3H; $CH_2CH_2CH_2$-CH_3). IR (KBr) ν/cm^{-1}: 3440 (N−H), 1675 (C=O), 843 (PF_6^-). Positive-ion ESI-MS ion cluster at m/z 810 $\{M - PF_6^-\}^+$. Anal. Calcd for $C_{37}H_{31}F_6IrN_9OP$: C, 46.54; H, 3.27; N, 13.20. Found: C, 46.47; H, 3.35; N, 13.44.

$[Ir(bzq)_2(dpq)](PF_6)$ (2a). Complex **2a** was isolated as orange crystals. Yield: 122 mg (66%). ^1H NMR (300 MHz, acetone-d_6, 298 K, TMS): δ = 9.73 (dd, J = 8.5, 1.5 Hz, 2H; H4, H4′ pyrido rings dpq), 9.33 (s, 2H; H2, H3 quinoxaline dpq), 8.54−8.50 (m, 4H; H6, H6′ pyrido rings dpq, H4 bzq), 8.26 (dd, J = 5.6, 1.2 Hz, 2H; H2 bzq), 8.11 (dd, J = 8.5, 5.2 Hz, 2H; H5, H5′ pyrido ring dpq), 8.00 (d, J = 8.8 Hz, 2H; H6 bzq), 7.88 (d, J = 8.8 Hz, 2H; H5 bzq), 7.59 (d, J = 7.9 Hz, 2H; H7 bzq), 7.44

(43) Perrin, D. D.; Armarego, W. L. F. *Purification of Laboratory Chemicals*; Pergamon: Oxford, 1997.
(44) Maniatis, T.; Fritsch, E. F.; Sambrook, J. *Molecular Cloning: A Laboratory Manual*; Cold Spring Harbor Laboratory: New York, 1982; p 458.
(45) Collins, J. G.; Sleeman, A. D.; Aldrich-Wright, J. R.; Greguric, I.; Hambley, T. W. *Inorg. Chem.* **1998**, *37*, 3133–3141.
(46) Delgadillo, A.; Romo, P.; Leiva, A. M.; Loeb, B. *Helv. Chim. Acta* **2003**, *86*, 2110–2120.
(47) Sprouse, S.; King, K. A.; Spellane, P. J.; Watts, R. J. *J. Am. Chem. Soc.* **1984**, *106*, 6647–6653.
(48) Demas, J. N.; Crosby, G. A. *J. Phys. Chem.* **1971**, *75*, 991–1024.
(49) Nakamura, K. *Bull. Chem. Soc. Jpn.* **1982**, *55*, 2697–2705.

(dd, J = 7.9, 5.3 Hz, 2H; H3 bzq), 7.23 (dd, J = 7.9, 7.3 Hz, 2H; H8 bzq), 6.48 (d, J = 7.0 Hz, 2H; H9 bzq). IR (KBr) ν/cm^{-1}: 845 (PF_6^-). Positive-ion ESI-MS ion cluster at m/z 781 $\{M - PF_6^-\}^+$. Anal. Calcd for $C_{40}H_{24}F_6IrN_6P$: C, 51.89; H, 2.61; N, 9.08. Found: C, 51.88; H, 2.80; N, 9.31.

[Ir(bzq)$_2$(dpqa)](PF$_6$) (2b). Complex **2b** was isolated as orange-yellow crystals. Yield: 123 mg (60%). ^{1}H NMR (300 MHz, acetone-d_6, 298 K, TMS): δ = 9.98 (dd, J = 8.5, 1.5 Hz, 1H; H4 pyrido ring dpqa), 9.71 (s, 1H; H3 quinoxaline dpqa), 9.59 (dd, J = 8.2, 1.5 Hz, 1H; H4′ pyrido ring dpqa), 9.08 (t, J = 6.5 Hz, 1H; NH), 8.54−8.48 (m, 4H; H6, H6′ pyrido rings dpqa, H4 bzq), 8.28 (dd, J = 5.0, 1.2 Hz, 2H; H2 bzq), 8.09−7.98 (m, 2H; H5, H5′ pyrido rings dpq), 7.97 (d, J = 8.8 Hz, 2H; H6 bzq), 7.85 (d, J = 8.8 Hz, 2H; H5 bzq), 7.55 (d, J = 7.9 Hz, 2H; H7 bzq), 7.47−7.42 (m, 2H; H3 bzq), 7.20 (t, J = 7.6 Hz, 2H; H8 bzq), 6.49 (d, J = 7.3 Hz, 2H; H9 bzq), 3.49 (q, J = 7.5 Hz, 2H; CH_2CH$_2$CH$_2$CH$_3$), 1.66 (quin, J = 7.5 Hz, 2H; CH$_2$CH_2CH$_2$CH$_3$), 1.40 (sext, J = 7.6 Hz, 2H; CH$_2$CH$_2$CH_2CH$_3$), 0.94 (t, J = 7.3 Hz, 3H; CH$_2$CH$_2$CH$_2$-CH_3). IR (KBr) ν/cm^{-1}: 3476 (N−H), 1681 (C═O), 847 (PF_6^-). Positive-ion ESI-MS ion cluster at m/z 880 $\{M - PF_6^-\}^+$. Anal. Calcd for $C_{45}H_{33}F_6IrN_7OP$: C, 52.73; H, 3.25; N, 9.57. Found: C, 52.49; H, 3.35; N, 9.80.

[Ir(pq)$_2$(dpq)](PF$_6$) (3a). Complex **3a** was isolated as orange crystals. Yield: 153 mg (78%). ^{1}H NMR (300 MHz, acetone-d_6, 298 K, TMS): δ = 9.64 (dd, J = 8.2, 1.5 Hz, 2H; H4, H4′ pyrido rings dpq), 9.20 (s, 2H; H2, H3 quinoxaline dpq), 8.87 (dd, J = 5.3, 1.5 Hz, 2H; H6, H6′ pyrido rings dpq), 8.58 (d, J = 8.8 Hz, 2H; H3 quinoline pq), 8.50 (d, J = 8.8 Hz, 2H; H4 quinoline pq), 8.34 (d, J = 8.2 Hz, 2H; H3 phenyl ring pq), 8.26 (dd, J = 8.2 and 5.3 Hz, 2H; H5, H5′ pyrido rings dpq), 7.80 (d, J = 8.2 Hz, 2H; H8 quinoline pq), 7.39 (d, J = 8.8 Hz, 2H; H5 quinoline pq), 7.29−7.23 (m, 4H; H6, H7 quinoline pq), 6.95−6.88 (m, 4H; H4, H5 phenyl ring pq), 6.70 (d, 2H; J = 7.6 Hz, H6 phenyl ring pq). IR (KBr) ν/cm^{-1}: 843 (PF_6^-). Positive-ion ESI-MS ion cluster at m/z 600 $\{M - PF_6^- - dpq\}^+$, 833 $\{M - PF_6^-\}^+$. Anal. Calcd for $C_{44}H_{28}F_6IrN_6P$: C, 54.04; H, 2.89; N, 8.59. Found: C, 54.25; H, 2.73; N, 8.80.

[Ir(pq)$_2$(dpqa)](PF$_6$) (3b). Complex **3b** was isolated as orange-red crystals. Yield: 162 mg (75%). ^{1}H NMR (300 MHz, acetone-d_6, 298 K, TMS): δ = 9.88 (dd, J = 8.2, 1.5 Hz, 1H; H4 pyrido ring dpqa), 9.69 (s, 1H; H3 quinoxaline dpq), 9.66 (dd, J = 8.2, 1.5 Hz, 1H; H4′ pyrido ring dpqa), 9.01 (t, J = 6.5 Hz, 1H; NH), 8.90 (dd, J = 5.3, 1.5 Hz, 1H; H6 pyrido ring dpq), 8.87 (dd, J = 5.3, 1.5 Hz, 1H; H6′ pyrido ring dpq), 8.58 (d, J = 8.8 Hz, 2H; H3 quinoline pq), 8.50 (d, J = 9.0 Hz, 2H; H4 quinoline pq), 8.35−8.23 (m, 4H; H5, H5′ pyrido rings dpq, H3 phenyl ring pq), 7.81 (d, J = 7.6 Hz, 2H; H8 quinoline pq), 7.44−7.35 (m, 2H; H5 quinoline pq), 7.28−7.22 (m, 4H; H6, H7 quinoline pq), 6.96−6.83 (m, 4H; H4, H5 phenyl ring pq), 6.70 (d, 2H; J = 7.6 Hz, H6 phenyl ring pq), 3.49 (q, J = 6.8 Hz, 2H; CH_2CH$_2$CH$_2$CH$_3$), 1.64 (quin, J = 7.5 Hz, 2H; CH$_2$CH_2CH$_2$CH$_3$), 1.41 (sext, J = 7.6 Hz, 2H; CH$_2$CH$_2$CH_2CH$_3$), 0.93 (t, J = 7.3 Hz, 3H; CH$_2$CH$_2$CH$_2$-CH_3). IR (KBr) ν/cm^{-1}: 3492 (N−H), 1683 (C═O), 843 (PF_6^-). Positive-ion ESI-MS ion cluster at m/z 600 $\{M - PF_6^- - dpqa\}^+$, 932 $\{M - PF_6^-\}^+$. Anal. Calcd for $C_{49}H_{37}F_6IrN_7OP \cdot CH_3COCH_3$: C, 55.02; H, 3.82; N, 8.64. Found: C, 55.01; H, 3.99; N, 8.88.

Crystal Structure Determination of Complex 3a. Single crystals of complex **3a** suitable for X-ray crystallographic studies were obtained by slow diffusion of petroleum ether (40−60 °C) vapor into a concentrated acetone solution of the complex. A crystal of dimensions 0.5 × 0.15 × 0.1 mm^3 mounted in a glass capillary was used for data collection at 28 °C on a MAR diffractometer with a 300 mm image plate detector using graphite monochromatized $Mo_{K\alpha}$ radiation (λ = 0.710 73 Å). Data collection was made with 2° oscillation steps of φ, 7 min exposure time and a scanner distance at 120 mm. A total of 100 images were collected. The images were interpreted and intensity integrated using the program DENZO.[50] The structure was solved by direct methods employing the program SHELXS-97 [51] on a PC. Iridium and many non-hydrogen atoms were located according to the direct methods. Positions of other non-hydrogen atoms were found after successful refinement by full-matrix least-squares using the program SHELXL-97.[51] One crystallographic asymmetric unit consists of one formula unit, including one hexafluorophosphate anion and one acetone molecule. In the final stage of least-squares refinement, non-hydrogen atoms of solvent molecules were refined isotropically, while other non-hydrogen atoms were refined anisotropically. Hydrogen atoms were generated by SHELXL-97. The positions of the hydrogen atoms were calculated based on riding mode with thermal parameters equal to 1.2 times that of the associated carbon atoms, and participated in the calculation of final R-indices. Crystal data and a summary of data collection and refinement details are given in Supporting Information, Table S2. CCDC-750895 contains the supplementary crystallographic data for this paper.

MTT Assays. HeLa or MDCK cells were seeded in a 96-well flat-bottomed microplate (10,000 cells/well) in growth medium (100 μL) and incubated at 37 °C under a 5% CO_2 atmosphere for 24 h. Detailed procedures for the cytotoxicity assays have been described previously.[21b] The absorbance of the solutions at 570 nm was measured with a SPECTRAmax 340 microplate reader (Molecular Devices Corp., Sunnyvale, CA). The IC_{50} values of the complexes were determined from dose dependence of surviving cells after exposure to the complexes for 48 h.

Live-Cell Confocal Imaging. MDCK cells were grown in a 35 mm glass bottom tissue culture dish and incubated at 37 °C under a 5% CO_2 atmosphere for 48 h. The culture medium was removed and replaced with CO_2-independence medium/DMSO (99:1, v/v) containing the complex at a concentration of 50 μM. In the following 3 h, imaging was performed using a confocal microscope (Leica TCS SP5) with an excitation wavelength at 488 nm. The emission was measured using a long-pass filter at 532 nm.

Fixed-Cell Confocal Imaging. MDCK cells were grown on sterile glass coverslips in a 60 mm tissue culture dish and incubated at 37 °C under a 5% CO_2 atmosphere for 48 h. The culture medium was removed and replaced with MeOH. After incubation for 5 min at 4 °C, the MeOH was removed, and the cell layer was washed gently with PBS (5 mL × 3) and then incubated with PBS/DMSO (99:1, v/v) containing the complex (5 μM, 30 min). After washing with PBS, the coverslips were mounted onto slides for measurements. Imaging experiments were performed using a confocal microscope (Leica TCS SPE) with an excitation wavelength at 405 nm. The emission was measured using a long-pass filter at 532 nm. In the costaining experiments, the fixed cells were incubated with fibrillarin antibody (20 μL/mL, 1 h), washed with PBS (5 mL × 3), incubated with Alexa 633 antirabbit IgG antibody (20 μg/mL, 30 min), washed with PBS (5 mL × 3), then incubated with PBS/DMSO (99:1, v/v) containing the complex (5 μM, 30 min). In the RNA-denaturation experiments, the fixed cells were treated with ribonuclease A (50 μg/mL, 1 h) and then incubated with PBS/DMSO (99:1, v/v) containing the complex (5 μM, 30 min).

Emission Titrations. In a typical experiment, the iridium(III) dpq or dpqa complex (10 μM) in buffer (50 mM, pH 7.4)/MeOH (2 mL, 7:3, v/v) was titrated with the BSA (2 mM) in potassium phosphate buffer (50 mM, pH 7.4), ds-CT-DNA (10 mM), or torula yeast RNA (20 mM) in Tris-Cl buffer (50 mM, pH 7.4)

(50) Otwinowski, Z.; Minor, W. DENZO Program In *Methods in Enzymology*; Academic Press: San Diego, CA, 1997; Vol. *276*, p 307.

(51) Sheldrick, G. M. *SHELXS-97 and SHELXL-97, Programs for Crystal Structure Analysis* (*Release 97-2*); University of Göttingen: Göttingen, Germany, 1997.

by additions of 5 μL aliquots of the titrant at 1 min intervals. The solution was excited at 350 nm, and the emission spectra at 450−850 nm were measured.

The binding constants ($K_{a,BSA}$) of the iridium(III) dpq and dpqa complexes to BSA were determined by the Hill equation:[52]

$$\log\{Y/(1-Y)\} = n_H \log[BSA] + n_H \log K_{a,BSA}$$

$$Y = (I_{obs} - I_{min})/(I_{max} - I_{min})$$

where I_{obs}, I_{min}, and I_{max} are the emission intensities of the apparent, free, and bound forms of the iridium(III) complex, respectively; n_H is the Hill coefficient.

The intrinsic binding constants ($K_{a,DNA}$) of the iridium(III) dpq and dpqa complexes to ds-CT-DNA were determined by using the following two equations developed by Bard[53] and Thorp:[54]

$$(I_a - I_f)/(I_b - I_f) = \{b - (b^2 - 2K_{a,DNA}{}^2 C_t[DNA]/s)^{1/2}\}/(2K_{a,DNA}C_t)$$

$$b = 1 + K_{a,DNA}C_t + K_{a,DNA}[DNA]/(2s)$$

where I_a is the emission intensity of the complex at a DNA concentration [DNA]; I_b is the emission intensity of the fully bound species; I_f is the emission intensity of free complex and C_t is the total concentration of the metal complex; s is the binding site size.

Protein Isolation and Electrophoresis. A 3 month old marine Medaka was anaesthetized by immersing in ice-cold water and sacrificed by beheading. The fish was then dissected, and the liver, gills, muscle, and skin were removed. HUVEC were maintained in HUVEC culture medium supplemented with 10% fetal bovine serum at 37 °C and 5% CO_2. The cells were harvested and fractionated into cytoplasm, nuclei, nucleoplasm, and nucleoli as described previously.[55] The tissues and cellular fractions were sonicated in SDS-sample buffer, heated according to the manufacturer's instruction, and then separated in a 10% Novex precast gel. For 2D gel electrophoresis, MDCK cells were directly lysed in 2D gel sample buffer according to manufacturer's instruction, and the extracted proteins were separated by the Ettan 2D gel apparatus. The gels were fixed in 50% MeOH with 10% acetic acid in water for 10 min, and then stained with complex **3a** (50 μM) for 30 min. The staining was examined by the Bio-Rad Gel Doc imager.

Acknowledgment. We thank The Hong Kong Research Grants Council (Project Nos. CityU 101908 and 102109) for financial support. K.Y.Z. and S.P.-Y.L. acknowledge the receipt of a postgraduate studentship administered by the City University of Hong Kong. K.Y.Z. acknowledges the receipt of research tuition scholarship and an outstanding academic performance award administered by the City University of Hong Kong.

Supporting Information Available: X-ray crystallographic data in CIF format, electronic absorption spectral data of all the complexes in CH_2Cl_2 and CH_3CN at 298 K, crystal data and a summary of data collection and refinement details, and concentration-effect curves for the MTT assays of all the complexes. This material is available free of charge via the Internet at http://pubs.acs.org.

(52) Yamada, Y.; Matsuura, K.; Kobayashi, K. *Bioorg. Med. Chem.* **2005**, *13*, 1913–1922.

(53) Carter, M. T.; Rodriguez, M.; Bard, A. J. *J. Am. Chem. Soc.* **1989**, *111*, 8901–8911.

(54) (a) Kalsbeck, W. A.; Thorp, H. H. *J. Am. Chem. Soc.* **1993**, *115*, 7146–7151. (b) Smith, S. R.; Neyhart, G. A.; Kalsbeck, W. A.; Thorp, H. H. *New J. Chem.* **1994**, *18*, 397–406.

(55) Lam, Y. W.; Lamond, A. I.; Mann, M.; Andersen., J. S. *Curr. Biol.* **2007**, *17*, 749–760.